Local Dynamics of Poly(ethylene oxide) in Solution. 1. Localization of Chain Motion

Michael M. Fuson*

Department of Chemistry and Biochemistry, Denison University, Granville, Ohio 43023

M. D. Ediger

Department of Chemistry, University of Wisconsin, 1101 University Avenue, Madison, Wisconsin 53706

Received January 14, 1997; Revised Manuscript Received July 18, 1997[⊗]

ABSTRACT: Fully atomistic molecular dynamics simulations have been performed on a solution consisting of a poly(ethylene oxide) (PEO) chain of 54 repeat units and 207 toluene molecules at 338 K and 1 bar. The local dynamics of the PEO chain have been examined. Equilibration in a given torsional potential well occurs in about 1.5 ps. Average conformational transition times are 7.4 and 9.0 ps for CO and CC torsions, respectively. Changes in atomic positions or torsional angles accompanying conformational transitions are localized within 8−10 atoms along the polymer chain, in good agreement with simulations of hydrocarbon polymers. About 15% of transitions are correlated with a second transition at the next-neighbor position. In addition to trans-centered cooperative transition pairs that have previously been observed in polyethylene simulations, a variety of types of gauche-centered pairs occur quite frequently.

I. Introduction

In this paper we report a study of the local dynamics of poly(ethylene oxide) (PEO) in dilute toluene solution using molecular dynamics simulations. Here we focus on the mechanism of local dynamics, e.g., characterizing the cooperativity of local chain motion. This is a topic of considerable recent interest and the present study is the first detailed consideration of a heteroatom polymer in solution. In the following paper[1] we focus on vector autocorrelation functions both in order to understand the mechanisms leading to loss of orientational order and as a way to characterize the anisotropy in the local dynamics. The anisotropy can be compared to the results obtained from NMR spin relaxation experiments.

CH vector reorientation and other local dynamic processes in polymers are usually conceptualized as occurring on three time scales: a very rapid relaxation due to librational motion about the current conformation (rotational isomeric state), a somewhat slower relaxation due to transitions between conformations, and finally slower relaxations associated with loss of orientational memory of larger portions of the polymer chain. The two faster processes are commonly characterized as "local dynamics" and are the focus of attention here. These local dynamics have an important influence on the macroscopic properties of polymer systems, including such technologically important properties as elasticity, glass transition temperatures, and the temperature dependence of melt viscosities.[2,3]

PEO has been chosen as the polymer to simulate both because of the considerable technological and biomedical importance of PEO and because it is one of a series of polyethers exhibiting a wide range of conformational and dynamic properties. For instance, poly(oxymethylene) strongly prefers gauche states, leading to helical local conformations, while polyethylene (which can be placed in the context of polyethers by considering it a polyether with an infinite number of methylenes between oxygens) adopts predominantly trans states and zigzag local conformations. PEO and poly(tetramethylene oxide) are intermediate in behavior.[4] NMR measurements of the local anisotropy of the dynamics of these polymers show a range of behaviors with poly(oxymethylene) showing the most *isotropic* local dynamics and polyethylene the most *anisotropic* local dynamics.[5−7] Simulations of other members of this series are underway. A toluene solution was chosen to allow direct comparisons of the current work to recent simulations of polyisoprene (PI) in toluene solution[8] and to avoid difficult issues about correctly simulating dynamics in a strongly hydrogen bonding solvent such as water.

Previous simulations of PEO in solution[9−12] and in the melt[13−15] have been reported. The simulations of PEO solutions have focused primarily on structural issues, such as differences between conformation in vacuum and with explicit water or benzene solvents. In his recent paper, Tasaki has included a brief examination of the local dynamics of a PEO 15mer in benzene and in water,[12] presenting calculations of conformational transition rates and of correlation times derived from both torsional and bond vector autocorrelation functions. For PEO melts an extensive comparison of simulated and observed NMR spin relaxation rates and dielectric relaxation has recently appeared,[14] but analysis of the molecular details of the polymer dynamics is still forthcoming.

In this paper we will address from a fresh perspective some fundamental issues regarding local dynamics that have been extensively investigated in hydrocarbon polymers. Recent simulations have examined the roles of librational motion, conformational transitions, correlation between conformational transitions, and coupling of librations in orientational relaxation in polymers.[17−25] We examine the roles of these processes in PEO with particular focus on understanding the mechanisms leading to localization of chain motion. Analysis of the local dynamics is commonly accomplished, on the one hand, by identifying specific molecular motions like torsional transitions or the degree of torsional "spreading" between transitions and alternatively by calculating P_1 or P_2 autocorrelation functions associated with various orientational or conformational properties. In

[⊗] Abstract published in *Advance ACS Abstracts,* September 1, 1997.

S0024-9297(97)00034-X CCC: $14.00

the present paper we shall focus exclusively on the former, reserving the latter for consideration in the following paper.[1]

II. Simulation Description

The molecular dynamics simulations described here were generated using *Discover 2.9.5* (Biosym Technologies, San Diego, CA) on a Silicon Graphics Power Challenge 4 workstation. A 54mer of PEO (2397 MW, 163 backbone atoms) was surrounded by 207 toluenes to give a system that is 11.2% polymer by weight. All atoms of both the polymer and the solvent were explicitly represented to give a total of 3486 atoms. The simulations were run with periodic boundary conditions under constant temperature and constant pressure using an 8 Å cutoff for nonbonded interactions. One femtosecond time steps were used in the calculation, but the atomic coordinates were saved only every 100 fs. Each of four starting configurations was run for a total of 1200 ps, with the final 990 ps of each run used for analysis. A single trajectory required about 10 days on a single R8000 processor.

Solvent Force Field. A slightly modified version of the Biosym force field *CFF91*[26] was used for the solvent. *CFF91* energies include contributions from bond stretching, bond bending, torsions, and cross-terms among all of these. Nonbonded interactions are modeled by a Lennard-Jones-like 6−9 potential and Coulombic partial charge terms. Following a suggestion of Suter,[27] r^* values for the nonbonded interactions were modified to give better agreement with the experimental density at 1 bar. Here, all r^* were reduced by 5.7%.

PEO Force Field. PEO is known to adopt primarily gauche conformations about its carbon−carbon bond.[28] This is an example of the "oxygen gauche effect." It is not reproduced well by commercial force fields.[29] For example, *CFF91* yields 76% trans CC bonds. We therefore adopted the force field for PEO developed by Smith, Jaffe and Yoon (SJY),[29] based on extensive *ab initio* electronic structure calculations on the model compound 1,2-dimethoxyethane (DME).[30] All parameters except nonbonded dispersion and repulsion were adopted without modification. SJY give the nonbonded interactions as

$$E^{\mathrm{NB}}(r_{ij}) = A_{ij}\mathrm{e}^{-r_{ij}B_{ij}} - C_{ij}r_{ij}^{-6} \qquad (1)$$

where r_{ij} is the distance between atoms i and j and A_{ij}, B_{ij}, and C_{ij} are parameters. *CFF91* implements the nonbonded interactions in the following form:

$$E^{\mathrm{NB}}(r_{ij}) = \epsilon_{ij}\left(2\left(\frac{r_{ij}^*}{r_{ij}}\right)^{-9} - 3\left(\frac{r_{ij}^*}{r_{ij}}\right)^{-6}\right) \qquad (2)$$

where r_{ij}^* is the internuclear separation at the potential minimum and ϵ_{ij} is the well depth. To reproduce the SJY nonbonded potential within the *CFF91* form, we performed a least squares fit of the *CFF91* form to the SJY potential, fitting at values of r_{ij} from where the SJY potential decreased below $3kT$ to 8 Å (the cutoff used in the simulations) and weighted by the relative importance of the type of interaction, that is by N_iN_j, where N_i is the number of atoms of type i in the polymer. The resulting parameters are given in Table 1. Table 2 gives the relative energies of various conformers and low lying conformational barriers of DME as calculated by electronic structure calculations, by the SJY force field, and by this work. The conformations listed are for the three central torsions in DME: about OC, CC, and CO bonds. The agreement is reasonable, especially for the lowest energy conformers.

Table 1. Nonbonded Force Field Parameters for PEO

atom (I)	r_{ii}^* (Å)	ϵ_{ii} (kcal mol^{-1})
C	4.243	0.005 69
H	3.746	0.002 20
O	3.209	0.231 1

Table 2. Energies of DME Conformers and Barriers (kcal mol^{-1})

	ab initio[a]	SJY[a]	this work
	Conformer		
ttt	0.00	0.00	0.00
tgt	0.15	0.14	0.13
tg$^{\pm}$g$^{\mp}$	0.23	0.19	0.28
ttg	1.43	1.38	1.20
tg$^{\pm}$g$^{\pm}$	1.51	1.74	1.62
g$^{\pm}$g$^{\pm}$g$^{\pm}$	1.64	3.19	2.84
g$^{\pm}$g$^{\pm}$g$^{\mp}$	1.86	1.70	1.65
g$^{\pm}$g$^{\mp}$g$^{\pm}$	2.41	2.07	2.50
g$^{\pm}$tg$^{\mp}$	3.08	2.64	2.29
g$^{\pm}$tg$^{\pm}$	3.13	2.66	2.29
tct	8.90	7.84	7.81
	Barrier		
ttt-tgt	2.31	1.88	1.81
ttt-ttg	2.04	1.97	1.98
ttg$^{\mp}$-tg$^{\pm}$g$^{\mp}$	2.03	2.48	1.58
tg$^{\pm}$t-tg$^{\pm}$g$^{\mp}$	1.36	1.41	1.62

[a] From ref 29.

Polymer Chain Generation. PEO chains were initially generated with random torsional angles using Biosym's *InsightII* and *Polymerizer* programs. The energy of the chains was then minimized for 100 steps to remove serious overlaps. Then the chains were subjected to brief vacuum molecular dynamics simulations according to the following temperature profile: heating from 0 to 1000 K over 1 ps, holding 10 ps at 1000K, cooling to 338 K over 4 ps, and holding 25 ps at 338K. Chain conformations that had root mean square end-to-end distances (R_e) and root mean square radii of gyration (R_g) approximately equal to those observed experimentally in solution were then chosen from the last 20 ps of the trajectories.

Solution Generation, Equilibration, and Trajectories. The polymer chains selected were placed in simulation boxes of preequilibrated solvent molecules, and any solvent molecules overlapping chain atoms were removed. After 100 steps of energy minimization, equilibration of the systems was begun by heating at constant volume over 1 ps to 1000 K followed by an additional 5 ps molecular dynamics at 1000 K at constant volume. Then the simulation conditions were changed to constant pressure at 4000 bar and continued for 5 ps more at 1000 K. (All pressures reported include the long-range correction due to potential energy truncation.[31]) Temperature and pressure were then reduced to 500 K and 1000 bar over 5 ps, followed by a slower cooling over 14 ps to the final temperature (338 K) and pressure (1 bar). The simulations were extended under these conditions for a total of 1200 ps. Solution and polymer properties such as density, potential energy, and torsional distributions appeared to achieve stable values by the end of 60 ps of equilibration. Nevertheless, we discarded the first 210 ps of each trajectory and the following analysis is based on the final 990 ps of each run. (A discussion of the adequacy of this equilibration scheme is in section III.) Using similar methods, a 180 ps trajectory of pure solvent (215 toluene

Table 3. Solvent Properties

	density (g/cm^3)	$10^9 D_t$ (m^2 s^{-1})	τ_c(ortho) (ps)	τ_c(meta) (ps)	τ_c(para) (ps)
expt	0.822[a]	4.54[b]	1.3[c]	1.3[c]	1.6[c]
toluene	0.814(8)	4.5(7)	0.95(10)	0.97(8)	1.26(9)
run 1	0.778(1)	5.9(2)	0.82(2)	0.81(1)	1.08(2)
run 2	0.778(1)	6.4(3)	0.83(2)	0.83(2)	1.08(2)
run 3	0.779(1)	5.9(3)	0.83(2)	0.84(2)	1.09(2)
run 4	0.780(1)	6.0(2)	0.85(2)	0.82(2)	1.09(2)

[a] From ref 34. [b] From ref 35. [c] Estimated from results at 298 K[8] using E_a.[36]

molecules) was also calculated for purposes of comparison.

Discover 2.9.5 Methodology. *Discover* implements the Verlet "leapfrog" algorithm to integrate Newton's equations of motion.[32] Temperature control is achieved by a velocity rescaling method that models the coupling of the system to a thermal reservoir.[33] Pressures are controlled by an analogous method that rescales the atomic coordinates and unit cell size.[33]

III. Solvent and Polymer Properties: Comparison to Experiment

Solvent Properties. In order to evaluate the reliability of the simulations we have calculated from the trajectories a number of the properties of the solvent that can be compared to experiment. In addition to the density, these include the toluene translational diffusion coefficient and the P_2 orientational autocorrelation times of the toluene aromatic CH bond vectors. The translational diffusion coefficient is calculated from the limiting slope of the mean square displacement of the centers of mass with respect to time:

$$D_t = \lim_{t\to\infty} \frac{1}{6} \frac{\mathrm{d}\langle r^2 \rangle}{\mathrm{d}t} \tag{3}$$

In practice, the mean square displacement as a function of time is calculated independently for each 30 ps section of the trajectory and the slope is taken from 7 to 22 ps. The bond vector correlation time is the time integral over the P_2 autocorrelation function of a unit vector pointing in the direction of the bond, e_{CH}:

$$\tau_c = \int_0^\infty \frac{1}{2} \langle 3(e_{CH}(0) \cdot e_{CH}(t))^2 - 1 \rangle \, \mathrm{d}t \tag{4}$$

Again, the correlation functions are calculated for each 30 ps section of the trajectory and are integrated numerically over the first 15 ps. Table 3 shows experimental values for pure toluene at 338 K (65 °C), values calculated from the 180 ps trajectory for the pure solvent, and values calculated for the solvent in the four solution trajectories. The values reported for the simulations are the averages of the values calculated independently for each 30 ps block of the trajectory. Uncertainties in the last digit are reported in parentheses and are standard errors.

The agreement between the simulated toluene density and the experimental density comes as no surprise as the force field was adjusted based on this parameter. The agreement between experimental and calculated translational diffusion coefficients is not forced, however, and is excellent. The computed bond correlation times are about 25% shorter than the experimental values derived from ^{2}H NMR spin relaxation experiments but show the correct relative magnitudes.

Table 4. Polymer Properties

	R_g (Å)	R_e (Å)
expt[a]	16	39
run 1	15.8(12)	36(6)
run 2	12.7(6)	20(3)
run 3	16.6(16)	36(4)
run 4	15.6(6)	34(3)
av	15.2	32

[a] Estimated from data in ref 38.

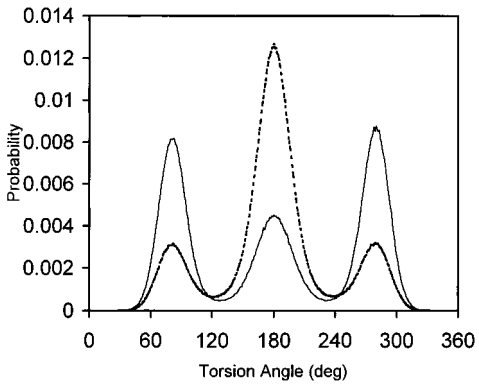

Figure 1. Population distributions for the torsion angles of PEO: (—) CC torsions;(- - -) CO torsions.

The solution density decreases from that of the pure solvent. Although we do not have experimental measurements with which to compare, this is the opposite effect from what would be expected. For instance, the density 10% PEO in benzene at 70 °C is 2.6% larger than that of pure benzene.[37] We attribute the behavior observed here to the very shallow well depths in the nonbonded interactions of the polymer atoms (see Table 1). So while the local conformational energies of the polymer are reproduced well, the overall solution is somewhat expanded. A consequence of this is seen in the solvent translational diffusion constant and bond vector correlation times which are somewhat faster in the solution simulations than in the pure solvent.

Polymer Properties. We have calculated several equilibrium properties of the polymer chains as simulated and compared them to experimental estimates. The polymer rms end-to-end distance, R_e, and rms radius of gyration, R_g, are summarized in Table 4. While the agreement is fairly good, it should be emphasized that the agreement is at least partially a function of our choice of initial conditions as the simulations reported here are not long enough to fully equilibrate large length scales such as the end-to-end distance.

Torsional angle distributions and conformer populations for single repeat units in the chain, on the other hand, are well sampled in these simulations. PEO has two types of torsions, about CC and CO bonds. The torsion angle distributions calculated from the average of all four runs are illustrated in Figure 1. A trans state is defined as 180°. As noted before, CC torsions are predominantly gauche (only 27% trans) while CO torsions are predominantly trans (69% trans). For both types of torsions the average gauche to trans barrier is low when compared to typical values for polymethylene chains. Here the barriers are 1.9−2.0 kcal/mol, calculated from the relative populations assuming a potential of mean force and using the Boltzmann distribution of energies.

Tasaki observed that during a simulation of a PEO 15mer in benzene at 300 K, beginning in the helical conformation characteristic of PEO in aqueous solution,

Table 5. PEO Conformer Solution Populations

conformer	PEO simulation	DME predicted[a]
ttt	0.147	0.144
tgt	0.303	0.248
$tg^{\pm}g^{\mp}$	0.299	0.408
ttg	0.104	0.066
$tg^{\pm}g^{\pm}$	0.080	0.061
$g^{\pm}g^{\pm}g^{\pm}$	0.006	0.025
$g^{\pm}g^{\pm}g^{\mp}$	0.038	0.036
$g^{\pm}g^{\mp}g^{\pm}$	0.002	0.008
$g^{\pm}tg^{\mp}$	0.010	0.003
$g^{\pm}tg^{\pm}$	0.011	0.003

[a] Estimated on the basis of the minimum energy of conformers as given in ref 30.

4 ns was required for the conformer populations to reequilibrate to stable values characteristic of a random coil.[12] In this context it makes sense to inquire whether the 210 ps equilibration time used here is sufficient to ensure that the local properties of the polymer under consideration here are fully equilibrated. The choice of an initial chain conformation with random angles and the brief high-temperature "annealings" were intended to make rapid equilibration possible. Examination of the torsion angle distribution (Figure 1) shows that there is no preference for one gauche conformation over the other, as was seen initially by Tasaki. Further, examination of the fraction of conformers in a given conformation as a function of time during the simulation (not shown) reveals only random fluctuation about a stable mean. Given the differences in the simulations, the fraction of bonds in trans conformers obtained here agrees reasonably well with those seen by Tasaki after equilibration (25% trans for CC, 74% trans for CO).[12] For these reasons we are confident that the local conformational populations are well equilibrated. Both conformational populations and local dynamic properties (such as conformational transition rates or correlation times, as discussed below and in the following paper[1]) show little variation among the four independent trajectories. Again, this is consistent with equilibration of the local properties of interest here.

Table 5 lists the fractional populations of three torsion sequences in the polymer (OC, CC, and CO) corresponding to single repeat units. The most commonly observed conformers are tgt and $tg^{\pm}g^{\mp}$, followed by ttt and ttg. The observed populations are consistent with those calculated from the *ab initio* energies of DME,[30] assuming a Boltzmann distribution (also given in Table 5). That the solution polymer conformations are consistent with predictions appropriate for the model compound in the gas phase is in accord with the available experimental evidence. Studies of the NMR vicinal coupling constants of DME in the gas phase[39] and DME and PEO in solution with various solvents[40] show that DME gas phase coupling constants are consistent with those of both DME and PEO in nonpolar solvents, accounting for differences in temperature. This would suggest similar conformer populations. Neat liquid DME and DME in polar solvents have distinctly different characteristics and recent molecular dynamics simulations of DME[41] suggest that this is due to a substantial shift in population from $tg^{\pm}g^{\mp}$ to tgt, a shift that is more modestly reflected here.

For the preceding analyses of torsion angle distributions and conformer populations, data regarding the last five repeat units from either end of the chain have been omitted in order to minimize end effects. This practice is followed throughout the following analysis of chain dynamics as well.

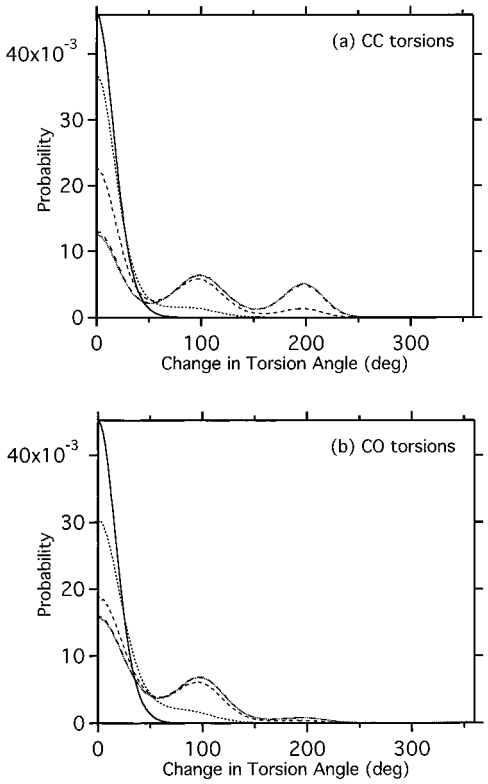

Figure 2. Probability of angular change $|\Delta\phi|$ for (a) CC torsion and (b) CO torsion at various time intervals: (—) 0.1 ps; (- - -) 1.0 ps; (— —) 10 ps; (— —) 100 ps; (···) 250 ps.

In the following paper[1] we compare correlation times for vector reorientation calculated from these trajectories to those obtained for NMR spin relaxation experiments. The results agree in absolute magnitude to within a factor of 2 or 3 and reproduce all trends in the data quite well.

IV. Torsional Dynamics and Conformational Transitions

Torsional Motion. We begin our consideration of the local dynamics of the polymer chain by examining torsional motion about a given main chain bond. Torsional motion can be characterized either by calculating the probability of a specified angular change in a given torsion angle at various times or by calculating appropriate torsional correlation functions. We will use the first approach.

Parts a and b of Figure 2 show the probability of an angular change $|\Delta\phi|$ during various time intervals for CC and CO torsions respectively. Within 0.1 ps, torsion angles have changed over a range of 0 to 60° in a distribution of probability that then changes very little in this angular range at longer times. At longer times new peaks grow in at 100 and 200°. The peak at 100° is fairly well developed at 10 ps and is similar for both CC and CO torsions. The peak at 200° is prominent only for CC torsions and develops at 100 ps.

These changes indicate dynamics on two different time scales. On short time scales, rapid motions establish an equilibrium distribution of angles within a torsional potential well. On longer time scales conformational transitions occur. A second transition at the same location and in the same direction occurs commonly for CC torsions only, because these torsions are primarily gauche and so can accomplish two consecutive transitions ($g^{\pm}$ to t to $g^{\mp}$) without encountering

Table 6. Barrier Crossings and Conformational Transitions

torsion	barrier crossings (ns^{-1})	transitions (ns^{-1})	fraction of successful barrier crossings	av transition time (ps)
CC	209(15)	111(6)	0.53	9.0
CO	275(5)	135(2)	0.49	7.4

the high $g^{\pm}$ to $g^{\mp}$ barrier. This barrier also makes rotation by 360° rare at even the longest times for either type of torsion. This behavior is qualitatively similar to that seen in simulations of PI in solution, although the time scales here are faster.[8]

Conformational Transitions. As noted above, the effects of conformational transitions are readily apparent in the distribution of torsion angle changes at times as small as 1 ps. To further quantify these events, we can tabulate their rates directly. We define a "conformational transition" as taking place when a torsion passes over a barrier and then continues past the minimum of the adjacent potential well. The time of the transition is defined as being the time at which the torsion crosses the barrier. Each torsion that crosses over the barrier and then returns to the original potential well without reaching the new minimum is tabulated as a single "barrier crossing". Positions of barriers and minima are taken from Figure 1. Average transition times and rates of barrier crossings and conformational transitions are given in Table 6.

As expected from Figure 2, conformational transitions are frequent, with a total of 66 376 observed in the four trajectories. The average transition times are less than 10 ps. One reason for this is the low gauche to trans barriers, as noted above. Another reason may be the relatively high fraction of barrier crossings that successfully continue on to become conformational transitions. For both types of transitions this fraction is approximately 0.5.

Another topic of interest is the degree of spatial heterogeneity of conformational transitions along the chain. Gee and Boyd have suggested that the ratio of the standard deviation in the number of transitions at a given bond to the average number of transitions, σ/N, is a useful way to characterize this heterogeneity.[20] For the simulations performed here this ratio is 0.11 for transitions about either CC or CO bonds, evaluated separately. In a completely homogeneous system σ would be $\sqrt{N}$, leading to σ/N having a value of $1/\sqrt{N}$ or 0.09 for the current simulation. Thus our system is quite close to this limit.

V. Localization of Chain Dynamics

The rapid time scales of local polymer dynamics require that the associated dynamic processes be localized in order to escape the large frictional forces associated with reorienting a large section of a polymer chain. Early consideration of this issue focused on rotational isomeric states, and localization was viewed as resulting from pairs of counter-rotating conformational transitions. More recent work has suggested that uncorrelated transitions accompanied by relaxation in neighboring torsional degrees of freedom are very important as well. These questions have been studied solely in hydrocarbon systems. In order to better understand the generality of the conclusions of previous studies, we examine these issues for PEO in solution. We begin by analyzing the degree of enhancement of chain motion in the neighborhood of a conformational transition. In the following section we then try to identify the proportion and type of cooperative transitions. The large number of conformational transitions observed in the present study allow rather detailed analysis.

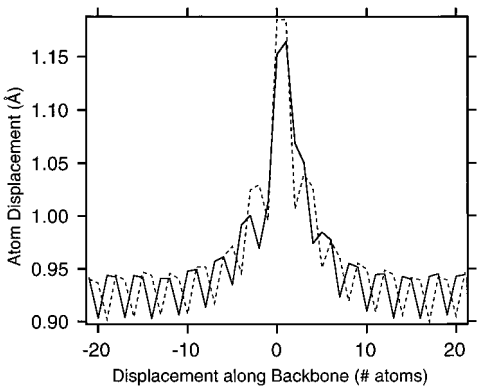

Figure 3. Average displacement of atomic coordinates accompanying a conformational transition at a CC torsion (- - -) or a CO torsion (—).

Atomic Displacements. A quite general way to assess the impact of conformational transitions on the local dynamics is to examine their effect on an appropriate parameter as a function of position relative to the position of the transition in space and time. In Figure 3 we show the average atomic displacement for backbone atoms near a conformational transition,

$$\langle |\vec{r}_i(\tau_{trans}+\Delta t) - \vec{r}_i(\tau_{trans}-\Delta t)| \rangle \qquad (5)$$

where r_i is the position of the backbone atom i away from the transition, τ_{trans} is the time of the transition, and Δt is chosen to be 0.2 ps. The displacements following transitions around CC and CO bonds are averaged separately. The numbering of the atoms is defined such that transitions take place between atoms 0 and 1. Maximum displacement is seen at the atoms adjacent to the transition, with those atoms moving about 0.2 Å further than atoms far enough from the transition to be at a baseline characteristic of motion in the absence of transitions. The extra displacement caused by transitions is quite localized, with the next atoms outward from the transition undergoing half or less of the perturbation seen adjacent to the transition. The perturbation disappears altogether about 10 atoms away from the transition. The "sawtooth" pattern observed in the baseline is due to the differing atomic masses of carbon and oxygen, with the heavier oxygens undergoing smaller average displacements. The choice of Δt used here maximizes the deviation of the average displacement from the background near the transition, but choosing Δt as long as 1 ps does not change the general features obtained. Overall, the pattern observed is quite similar to that seen in simulations of PI solutions and melts.[8,24]

Torsional Displacements. The average displacements in torsional coordinates near a conformational transition can also be calculated. Figure 4 shows the results of calculating the coherent torsional coupling, that is, the average displacement of a torsional coordinate ϕ in the *same direction* as a triggering conformational transition:

$$\langle A(\Delta\phi)|\phi(\tau_{trans}+\Delta t) - \phi(\tau_{trans}-\Delta t)| \rangle \qquad (6)$$

where Δt equals 0.2 ps and $A(\Delta\phi)$ is +1 if the torsion corotates with the triggering transition and is −1 for a

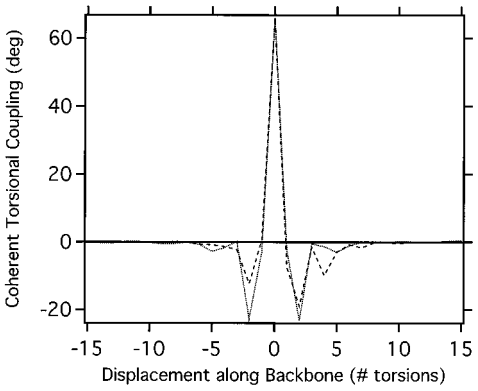

Figure 4. Average change in torsional angles accompanying a conformational transition for CC torsions (—) and CO torsions (- - -). The transition is at position zero. Negative angles represent counter-rotations.

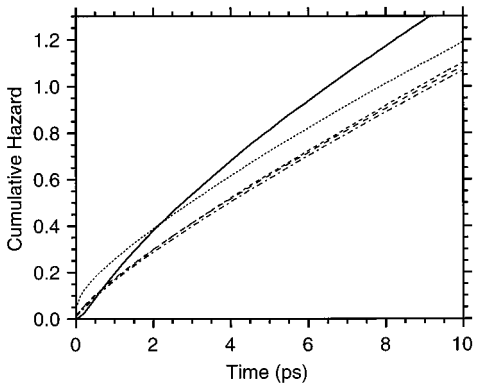

Figure 5. Cumulative hazard plots for both CC and CO torsions for back-transitions (—) and transitions at first (—•—), second (•••), third (- - -), and fourth (— — —) neighbors of the triggering transition.

Table 7. Hazard Function Parameters

neighbor	λ_i (ps^{-1})	ν_i	σ_i (ps)	c_i	fraction based on polynomial intercept
0	0.0956(18)	0.474(23)	4.02(17)	0.38	0.05
1	0.0928(4)	0.147(3)	1.62(6)	0.14	0.07
2	0.0995(7)	0.214(5)	0.681(5)	0.19	0.14
3	0.0961(5)	0.148(4)	1.50(7)	0.14	0.07
4	0.0942(4)	0.150(3)	1.39(6)	0.14	0.06

counter-rotation. Thus, the average will be positive if, on average, the selected torsion corotates with the triggering transition, negative if it counter-rotates, and zero if both possibilities are equally probable. In Figure 4 the large peak at zero displacement is simply the rotation of the triggering transition in the selected time increment. Significant counter-rotations can be seen at torsions ±2 from the triggering transition. These are similar to those previously seen for alkane systems. Weaker counter-rotations are apparent at +4 torsions for CO and at ±5 torsions for the CC torsion. All of these more distant correlated rotations occur at CO torsions. There are no significant torsional couplings at more than 6 or 7 torsions from the triggering transitions. As with the atomic displacements in the neighborhood of a transition, the calculated coherent torsional couplings indicate that the dynamic processes associated with conformational transitions are localized within about 3 repeat units on either side of the transition for PEO in solution.

VI. Correlation of Conformational Transitions

As noted above, one proposed mechanism of localization of the chain motion associated with conformational transitions is for a second "correlated" or "cooperative" transition to take place nearby in space and time to the original transition in order to minimize overall chain reorientation. The preceding analyses make no assumptions about the role or importance of correlated conformational transitions in localizing dynamic processes. In order to consider these issues, we shall utilize the cumulative hazard analysis introduced by Helfand[42] and the first failure pair analysis suggested by Boyd and co-workers.[19]

Hazard Analysis. The cumulative hazard is calculated from the set of first passage times, that is the times between a triggering transition for a given torsion and the first subsequent transition for a selected nearby torsion, arranged in increasing order. The "hazard", $h(t)\,dt$, is then the probability that a torsion will undergo its first transition between t and $t + dt$ after the triggering transition. The cumulative hazard is then the integral from zero to t of $h(t)\,dt$:

$$H(t) = \int_0^t h(t')\,dt' \tag{7}$$

If the transitions are uncorrelated and follow Poisson statistics, then a plot of the cumulative hazard versus time should be linear, with the slope giving the transition rate. Correlated transitions introduce curvature into the plot. Plots of the cumulative hazard for torsions 0−4 (where transitions at torsion 0 are back-transitions of the triggering torsion) are given in Figure 5. The plot of cumulative hazard for second neighbors shows the effect of correlation most clearly, with a steep rise at short times. The plots for all other torsions except back-transitions are less significantly curved. The plot for back-transitions shows distinct curvature on a much longer time scale than the near neighbors. This delay may be in part due to the definition of a "transition" used in this study. A transition is defined as crossing a barrier and proceeding to the minimum of the adjacent potential well. Half of all barrier crossings do not continue on to the minimum, and these rapid recrossings are not represented here. Requiring that a transition continue all the way to the bottom of a well may delay its subsequent transitions relative to neighboring torsions that may be positioned closer to their respective barriers.

In an attempt to quantify the cooperativity of the transitions, other workers have fit the cumulative hazard to the following form:[17,21]

$$H_i(t) = \lambda_i t + \nu_i(1 - e^{-t/\sigma_i}) \tag{8}$$

where the subscript i indicates we are considering the hazard to a torsion i torsions away from the triggering transition, λ_i is the rate of uncorrelated transitions, σ_i characterizes the spread in time of the correlated transitions, and ν_i is related to the fraction of transitions at torsion i that are correlated to the triggering transition, c_i,

$$c_i = 1 - e^{-\nu_i} \tag{9}$$

if $\sigma_i \ll 1/\lambda_i$. Parameters obtained by least squares fits of the first 10 ps of the cumulative hazard to eq 8 are given in Table 7.

While the results obtained are qualitatively very similar to those obtained for the C_{44} melt,[21] several

aspects of these results suggest they may not be quantitatively reliable. First, the separation of time scales, $\sigma_i \ll 1/\lambda_i$, assumed in calculating the fractions of cooperative transitions, c_i, is not clearly satisfied, particularly for c_0. Secondly, the fraction of cooperative transitions at each neighbor should sum to give the total fraction of transitions correlated with a given triggering transition. Here, summing the c_i gives 0.99; that is, on average, every transition is correlated with another one. This seems quite unlikely given that the average transition times are 8−9 ps, while the σ values obtained are much smaller. This problem is amplified if one considers a wider range of near neighbors. For example, the fifth through eighth neighbors (not shown) behave similarly to the fourth neighbor. A final problem is that the parameters obtained depend on the range of time of the cumulative hazard function that is fit. Very different parameters are obtained if a longer section such as 50 ps is used in the fitting procedure. This means that the long time behavior of the cumulative hazard is not truly linear and that the transitions are not a Poisson process at long times. Long time curvature of the cumulative hazard has been observed before.[16]

An *ad hoc* procedure for estimating the fraction of cooperative transitions can be constructed if we assume that the long time behavior of the cumulative hazard can be used to extrapolate back to an intercept at $t = 0$, which then represents the fraction of cooperative events. We have fit the cumulative hazard between 2 and 50 ps to a sixth-order polynomial. The resulting extrapolated intercepts are reported in the final column of Table 7. Increases in the order of the polynomial or the short time cutoff of the section used in the fit have small effects on the results obtained. The estimates of the fraction of cooperative transitions obtained in this manner reflect the same qualitative trends for the near neighbors, although at lower absolute numbers. Second neighbors show enhanced cooperativity relative to other near neighbors. The estimate of the cooperative fraction of back-transitions is much lower, however, and now similar to the first, third, and fourth near neighbors. A low fraction of back-transitions has also been seen in Brownian dynamics studies of polyethylene chains, where the time scales of random and cooperative transitions were well separated.[16]

First Failure Pair Analysis. An alternative method of describing the cooperativity of conformational transitions is first failure pair analysis.[19] Here, a specified range of torsions is searched for the first transition following a triggering transition. No time cutoff is imposed. Except at the beginning and end of the trajectories every transition can appear in more than one first failure pair, once as the triggering transition and again as the site of first failure. The results presented in Figure 6 are obtained when we examine back-transitions and ±8 nearest neighbors for transitions occurring at both CC and CO torsions. The cutoff of ±8 torsions is chosen based on the disappearance of any coherent torsional coupling at this length scale (see Figure 4). As was seen in the cumulative hazard analysis, second neighbor transitions are clearly more likely than either back-transitions or transitions at other near neighbors. If we take the fraction of first failures occurring at the eighth neighbor as representative of the background of random transitions found at every site, then about 16% of all transitions are correlated with a second neighbor and 25% are correlated

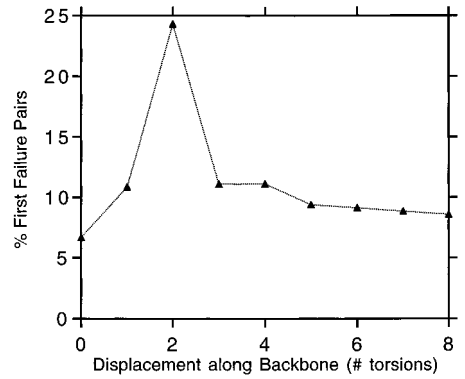

Figure 6. Symmetrized spatial location along the chain of the first conformational transition that follows a triggering transition at position 0 (first failure pairs).

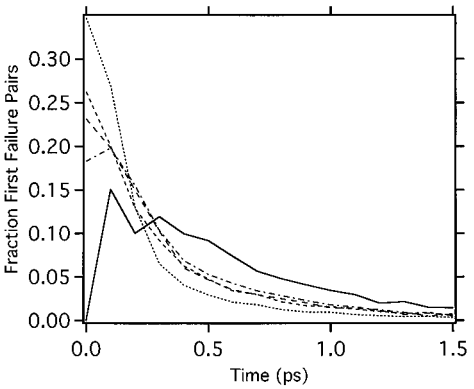

Figure 7. Probability distributions of times of first failures for back-transitions (—) and transitions at first (—•—), second (•••), third (- - -), and fourth (— — —) neighbors of the triggering transition.

with a neighbor within 8 torsions. While first failures at the site of the original transition appear in Figure 6 to have a reduced probability relative to near neighbors, this is misleading because first failures at a given near neighbor can occur at two sites, one on either side of the original transition, while back-transitions are confined to the single site of the original transition. Accounting for this difference, there are 2−3% more first failures occurring as back-transitions than expected from the background.

In Figure 7 we present the probability distribution of times of first failures at the original torsion and the four nearest neighbors. Each curve is normalized independently. 78% of all first failures take place in the first 0.5 ps after a triggering transition. This compares to a 66% probability of having a transition in a 17 torsion sequence in 0.5 ps if each torsion was independently following first-order kinetics, or a 12% enhancement. By 1 ps these values are 91% and 89%, respectively, and so any enhancement of the transition rate due to cooperativity effects has almost disappeared. As was seen in the hazard analysis, transitions at the second nearest neighbors occur more rapidly after a triggering transition than most near neighbors. Back transitions occur more slowly, probably for the reasons discussed above.

Types of First Failure Pairs. We have also analyzed the types of first failure pairs that occur in an effort to identify transition pairs involved in correlated motions. We begin with a fairly coarse-grained approach, grouping types of first failures according to the transitions occurring and ignoring the conformations of intervening torsions. This allows us to apply the

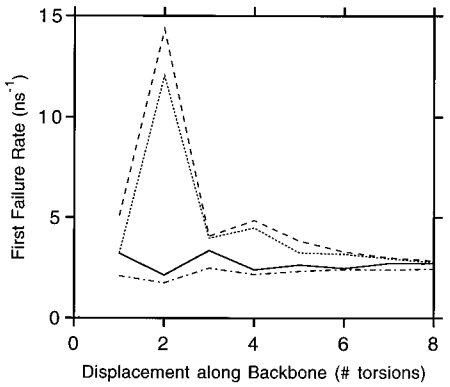

Figure 8. Rates of formation of various types of first failure pairs: $t^*g^{\pm} \rightleftarrows g^{\pm}{}^*t$ (- - -); $t^*t \rightleftarrows g^{\pm}{}^*g^{\mp}$ (•••); $t^*g^{\pm} \rightleftarrows g^{\mp}{}^*t$ (—); and $t^*t \rightleftarrows g^{\pm}{}^*g^{\pm}$ (—•—).

analysis identically for all neighbors and avoids the proliferation of conformations as the sequence of torsions under consideration lengthens. (Back transitions do not fit into this grouping and will be discussed below.) Grouped in this way, there are eight possible types of first failure pairs. Four involve only gauche to trans transitions and are fairly common: $t^*g^{\pm} \rightleftarrows g^{\pm}{}^*t$, $t^*t \rightleftarrows g^{\pm}{}^*g^{\mp}$, $t^*g^{\pm} \rightleftarrows g^{\mp}{}^*t$, and $t^*t \rightleftarrows g^{\pm}{}^*g^{\pm}$ where the asterisk represents the intervening sequence. The other four types of first failure pairs involve gauche to gauche transitions and are very rare in the simulations reported here. For second neighbors, if the central torsion is trans, then the first two types defined above correspond to "gauche migration" and "kink creation (or annihilation)" events identified as important in polymethylene dynamics.[16] In the same spirit, the third type can be described as "gauche migration with inversion" and the fourth as "bend creation (or annihilation)".

Figure 8 presents the rates of formation of the four common types of first failure pairs as a function of displacement along the backbone of the second transition from the triggering transition. The rates are given in first failure pair formation events per triggering torsion per nanosecond and can be compared to the total transition rates in Table 6. Gauche migration and kink creation rates are strongly elevated for second neighbors, paralleling the enhancement in total first failures seen in Figure 6. A modest peak for these rates is also seen at the fourth neighbor, and then they converge with the rates exhibited by the other two types of pairs at the eighth neighbor. This convergence suggests that the rate of formation of the various types of first failure pairs seen at this point represents the rate characteristic of random, uncorrelated events and supports the interpretation used in Figure 6 to extract the fraction of cooperative transitions.

The behavior of the rates of gauche migration with inversion and bend creation events is also interesting. For near neighbors bend creation rates are depressed by about 20% from the rates seen for far neighbors. This seems understandable given the degree of reorientation of the chain that would seem necessary to accommodate the creation or annihilation of two nearby and corotating gauche bonds. Even more interesting is the behavior of the rate of gauche migration with inversion events, because while this rate is depressed 20% for second neighbors, it is elevated 20% for first and third neighbors. Evidently, reorganization of neighboring torsions not involving crossing over into new conformational wells is able to accommodate such a pair of transitions for first and third neighbors. It is important to note

Table 8. PEO First Failure Rates (ns^{-1})

back-transitions	CC	CO
$t \rightarrow g^{\pm} \rightarrow t$	2.56	6.94
$g^{\pm} \rightarrow t \rightarrow g^{\pm}$	2.79	2.97
$g^{\pm} \rightarrow g^{\mp} \rightarrow g^{\pm}$	0.03	0.01
first neighbors	**CCO**	**COC**
$tg^{\pm} \rightleftarrows g^{\pm}t$	3.94	7.40
$tt \rightleftarrows g^{\pm}g^{\mp}$	4.38	0.90
$tg^{\pm} \rightleftarrows g^{\mp}t$	3.51	2.63
$tt \rightleftarrows g^{\pm}g^{\pm}$	2.24	1.77
all others (4 types)	0.05	0.03
second neighbors	**OCCO**	**CCOC**
$ttg^{\pm} \rightleftarrows g^{\pm}tt$	6.04	14.33
$ttt \rightleftarrows g^{\pm}tg^{\mp}$	5.29	13.63
$g^{\pm}g^{\mp}t \rightleftarrows tg^{\mp}g^{\pm}$	7.07	0.20
$g^{\pm}g^{\pm}t \rightleftarrows tg^{\pm}g^{\mp}$	3.36	0.74
$tg^{\pm}t \rightleftarrows g^{\pm}g^{\pm}g^{\mp}$	2.48	0.57
$tg^{\pm}t \rightleftarrows g^{\pm}g^{\pm}g^{\pm}$	1.27	0.96
all others (14 types)	1.82	1.76

that while the changes in rate discussed here are small, they are reproducible among the four trajectories and represent differences in the number of failure pairs of that type of about 300 events.

A more detailed analysis of the types of first failure pairs is possible for first failure pairs that occur at the original torsion and first and second neighbors. Because of the limited number of possible conformations, we can tabulate the rates of occurrence as a function of their specific initial and final conformations and in addition separate events at CC and CO torsions. These results are tabulated in Table 8. CCO stands for a CC torsion next to a CO torsion, etc.

Almost all back-transitions occur between gauche and trans conformations. This reflects the relative heights of the gauche−trans and gauche−gauche barriers. While the relative rates of $t \rightarrow g^{\pm} \rightarrow t$ back-transitions at CO and CC torsions reflect the ratio of these torsions initially found in the trans state, this is not the case for $g^{\pm} \rightarrow t \rightarrow g^{\pm}$ pairs, where CC torsions show a rate that is slower by a factor of 2 than might have been expected. Since total transition rates for CO and CC torsions are similar, this may signify that gauche to trans transitions at CC torsions are more efficiently coupled to some other first failure process, probably gauche migration and kink creation at CCOC second neighbor sequences, as discussed below. Any enhancement in first failure rates due to cooperative back-transitions would seem to be associated with CO torsions.

For first neighbors the types of failure pairs parallel exactly the general classes discussed above, with no intervening torsions. The data presented in Table 8 are the same as presented in Figure 8 except that transitions associated with CCO and COC sequences are separated. These data show that the rate of first failure can depend rather dramatically on both the type of failure and on the sequence of bonds. On the one hand, gauche migration rates are enhanced by a factor of 2 for COC sequences as compared to CCO sequences, with both above background levels (which are approximately 2.7 ns^{-1}). Kink creation rates, on the other hand, are enhanced for CCO sequences and greatly depressed for COC sequences, leading to a difference of a factor of 4 in rates.

Second neighbor first failure pairs centered on CO torsions, i.e., CCOC sequences, show polymethylene-like behavior: kink creation and gauche migration events

are very frequent, and no other pair appears at even one-tenth the rate. In contrast, OCCO sequences centered on a CC torsion exhibit a much wider range of types of pair formation. In addition to the two dominant types of transition pairs seen for CCOC sequences, four additional types are seen with reasonable rates, all with gauche torsions at the central CC torsion (recall that CC torsions are predominantly gauche). The four types are gauche-centered equivalents of the kink creation and gauche migration pairs and also of the gauche migration with inversion and bend creation discussed earlier.

In summary, 25−40% of transitions have a second transition correlated with them. Two separate lines of analysis suggest that about 15% of transitions are correlated with a second neighbor transition, with gauche migration and kink creation/annihilation events at CCOC sequences dominant. Analysis of the details of correlated transition pairs shows that although overall transition rates of CC and CO torsions are similar, fairly substantial differences can be seen in the rates of different types of transition pairs and for different bond sequences.

VII. Coupled Librations

Vector autocorrelation functions often show a rapid initial decay due to librational motion within a torsional potential well. Subsequent correlation function decay is often considered to be due to the effect of conformational transitions. Moe and Ediger, in their analysis of PI melt, solution, and vacuum simulations,[25] see evidence for additional mechanisms leading to correlation function decay. They considered the question of what motions lead to the continued decay of correlation functions calculated in regions of the trajectories between conformational transitions and on time scales long compared to libration within a single potential well.[25] This type of correlation function decay is seen in the current simulations of PEO solutions as well (see following paper[1]). Moe and Ediger propose that in these regions the important process is for groups of torsions to move cooperatively so that small angular motions in many individual torsions add up to a large vector reorientation, a process referred to as "coupled libration" by Moro.[43] To characterize this process they calculate

$$\langle | \sum_{m=1}^{n} \Delta\phi_m(t) | \rangle \qquad (10)$$

where n is the number of contiguous torsions considered in the calculation and $\Delta\phi_m(t)$ is the angular change of torsion m in time t. We present the results of a similar calculation in Figure 9a, modified in that the calculation is done only for those regions of the trajectories *between* conformational transitions instead of the entire trajectories. These regions are defined by excluding from consideration sections of the trajectories extending four methylenes to either side of a conformational transition and extending from 0.5 ps before a transition to 0.5 ps afterward. The curve for $n = 1$ is simply the absolute value of the average angular change of single torsions as a function of time. This reaches a plateau in about 1.5 ps and represents the time required for a single torsion to fully equilibrate. Larger groups of torsions show a rapid initial rise followed by a much more gradual continued increase.

Figure 9b shows the curves from Figure 9a normalized by dividing through by the curve for $n = 1$. If the motion of each torsion were uncorrelated with its neighbors, the value of the average normalized angular displacement would be $\sqrt{n}$ (the random walk result; here: 1.41, 2.24, and 3.16 respectively). The curve for $n = 2$ achieves this limit almost immediately. Larger groups of torsions begin below the random walk limit, indicating that groups of torsions tend to move in opposite senses on a picosecond time scale, localizing chain motions. This correlation of torsional rotations does not persist very long, however. It is interesting that if you linearly extrapolate the curve for $n = 5$, it reaches its random walk limit at about 10 ps, a time similar to the average conformational transition time. To reach this random walk limit the sum of torsional angle changes must reach 39°, which leads to a substantial reduction in the P_2 correlation function. Thus, CH bond vector correlation functions, whose time scales are closely associated with those of torsional correlation functions, can decay significantly even in the absence of conformational transitions. This will be illustrated in the following paper.[1]

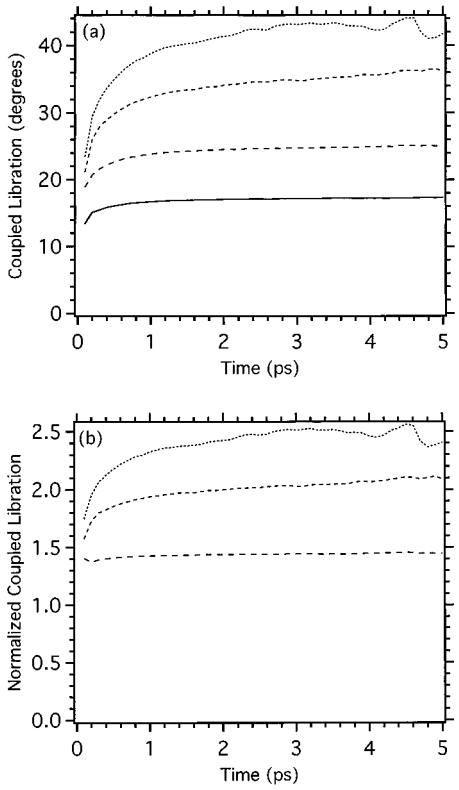

Figure 9. (a) Collective angular motion of groups of 1 (—), 2 (– – –), 5 (- - -), and 10 (···) torsions. (b) Same as (a) except normalized by the motion of a single torsion.

VIII. Concluding Remarks

In this paper we have described molecular dynamics simulations of the heteroatom polymer poly(ethylene oxide) in toluene solution. We have examined the extent and mechanism of localization of the chain dynamics.

For PEO, librational motion causes equilibration within a given torsional potential well in about 1.5 ps. Conformational transitions take place frequently, with average times between transitions of 7.4 and 9.0 ps for CO and CC torsions, respectively. Coupled librations between conformational transitions are sufficient to cause substantial chain reorientation on time scales comparable to average conformational transition times.

Calculations of the atomic or torsion angle displacement accompanying conformational transitions shows

that the perturbations to the local structure associated with conformational transitions are localized to within 8−10 atoms along the polymer chain. The localization of the motion associated with a conformational transition occurs either by a second conformational transition or by relaxation in neighboring torsions not involving a conformational transition. Estimating the fraction of transitions involved in cooperative pairs is difficult, but two separate lines of analysis suggest that about 15% of transitions are accompanied by cooperative second neighbor transitions. Altogether, 25−40% of transitions may be involved in cooperative pairs. These results are quite consistent with those obtained in earlier simulations of hydrocarbon polymers.

Although the total rates of occurrence of first failure pairs at different bond sequences for a given neighbor are usually fairly similar (for example, rates at OCCO and CCOC sequences for second neighbors differ by 15%), the rates for a given type of transition pair at the two different sequences are sometimes drastically different (as large as a factor of 35 for $g^{\pm}g^{\mp}t \rightleftarrows tg^{\mp}g^{\pm}$). Differences of about a factor of 2 may be explained by differences in overall transition rates at CC and CO torsions (18%) and by differences in the populations of given conformers (27% trans at CC; 69% trans at CO). Larger differences in rates are not easily understood. Nor are relatively high rates for transition pairs which would appear to involve large chain reorientations such as $g^{\pm}g^{\pm}t \rightleftarrows tg^{\pm}g^{\mp}$. Transitions involving apparent large chain reorientations have also been observed in simulations of *cis*-1,4-polybutadiene.[20]

In the following paper we examine vector correlation functions and the anisotropy of the local dynamics for PEO in solution using the molecular dynamics simulations presented here.[1] There we analyze the influence of conformational transitions on the anisotropy of the local dynamics.

Acknowledgment. The authors gratefully acknowledge many helpful conversations with Neil E. Moe. This work was supported in part by the National Science Foundation (DMR-9424472; M.D.E.). The computers used in this work were also purchased through a grant from the NSF (CHE-9522057). M.M.F. also acknowledges the support of an R. C. Good Fellowship from Denison University.

References and Notes

(1) Fuson, M. M.; Hanser, K. H.; Ediger, M. D. *Macromolecules* **1997**, *30*, 5714.
(2) Ferry, J. D. *Macromolecules* **1991**, *24*, 5237.
(3) Monnerie, L. *Makromol. Chem., Macromol. Symp.* **1991**, *48−49*, 125.
(4) Mark, J. E. *Acc. Chem. Res.* **1979**, *12*, 49.
(5) Fuson, M. M.; Anderson, D. J.; Liu, F.; Grant, D. M. *Macromolecules* **1991**, *24*, 2594.
(6) Fuson, M. M.; Miller, J. B. *Macromolecules* **1993**, *26*, 3218.
(7) Fuson, M. M.; Klei, B. R. *Macromolecules* **1996**, *29*, 5223.
(8) Moe, N. E.; Ediger, M. D. *Macromolecules* **1995**, *28*, 2329.
(9) Depner, M.; Schurmann, B. L.; Auriemma, F. *Mol. Phys.* **1991**, *74*, 715.
(10) Schurmann, B. L. *Polym. Prepr. (Am. Chem. Soc., Div. Polym. Chem.)* **1992**, *33*, 568.
(11) Tasaki, K. *J. Am. Chem. Soc.* **1996**, *118*, 8459.
(12) Tasaki, K. *Macromolecules* **1996**, *29*, 8922.
(13) Smith, G. D.; Yoon, D. Y.; Jaffe, R. L.; Colby, R. H.; Krishnamoorti, R.; Fetters, L. J. *Macromolecules* **1995**, *28*, 5897.
(14) Smith, G. D.; Yoon, D. L.; Wade, C. G.; O'Leary, D.; Chen, A.; Jaffe, R. L. *J. Chem. Phys.* **1997**, *106*, 3798.
(15) Neyertz, S.; Brown, D. *J. Chem. Phys.* **1995**, *102*, 9725.
(16) Weber, T. A.; Helfand, E. *J. Chem. Phys.* **1983**, *78*, 2881. Hall, C. K.; Helfand, E. *J. Chem. Phys.* **1982**, *77*, 3275.
(17) Takeuchi, H.; Roe, R.-J. *J. Chem. Phys.* **1991**, *94*, 7446.
(18) Adolf, D. B.; Ediger, M. D. *Macromolecules* **1991**, *24*, 5834. Ediger, M. D.; Adolf, D. B. *Macromolecules* **1992**, *25*, 1074.
(19) Boyd, R. H.; Gee, R. H.; Han, J.; Jin, Y. *J. Chem. Phys.* **1994**, *101*, 788.
(20) Gee, R. H.; Boyd, R. H. *J. Chem. Phys.* **1994**, *101*, 8028.
(21) Smith, G. D.; Yoon, D. Y.; Zhu, W.; Ediger, M. D. *Macromolecules* **1994**, *27*, 5563.
(22) Smith, G. D.; Yoon, D. Y.; Jaffe, R. L. *Macromolecules* **1995**, *28*, 5897.
(23) Kim, E.-G.; Mattice, W. L. *J. Chem. Phys.* **1994**, *101*, 6242.
(24) Moe, N. E.; Ediger, M. D. *Polymer* **1996**, *37*, 1787.
(25) Moe, N. E.; Ediger, M. D. *Macromolecules* **1996**, *29*, 5484.
(26) Maple, J. R.; Dinur, U.; Hagler, A. T. *Proc. Natl. Acad. Sci. U.S.A.* **1988**, *85*, 5350. Maple, J. R.; Thatcher, Y. S.; Dinur, U.; Hagler, A. T. *Chem. Des. Automat. News* **1990**, *5* (9), 5.
(27) Leontidis, E.; Suter, U. W.; Schutz, M.; Luthi, H.-P.; Renn, A.; Wild, U. P. *J. Am. Chem. Soc.* **1995**, *117*, 7493.
(28) Mark, J. E.; Flory, P. J. *J. Am. Chem. Soc.* **1965**, *87*, 1415. Mark, J. E.; Flory, P. J. *J. Am. Chem. Soc.* **1966**, *88*, 3702.
(29) Smith, G. D.; Jaffe, R. L.; Yoon, D. Y. *J. Phys. Chem.* **1993**, *97*, 12752.
(30) Jaffe, R. L.; Smith, G. D.; Yoon, D. Y. *J. Phys. Chem.* **1993**, *97*, 12745.
(31) Allen, M. P.; Tildesley, D. J. *Computer Simulation of Liquids*; Oxford: New York, 1987.
(32) Verlet, L. *Phys. Rev.* **1967**, *159*, 98.
(33) Berendsen, H. J. C.; Postma, J. P. M.; van Gunsteren, W. F.; DiNola, A.; Haak, J. R. *J. Chem. Phys.* **1984**, *81*, 3684.
(34) Egloff, G. *Physical Constants of Hydrocarbons*; Reinhold: New York, 1946; Vol. III, p 48.
(35) Pickup, S.; Blum, F. D. *Macromolecules* **1989**, *22*, 3961.
(36) Liu, G.; Mackowiak, Y.; Jonas, J. *J. Chem. Phys.* **1991**, *94*, 239.
(37) Booth, C.; Devoy, C. J. *Polymer* **1971**, *12*, 309.
(38) *Polymer Handbook*, 3rd ed.; Brandrup, J.; Immergut, E. H., Eds.; Wiley: New York, 1989.
(39) Inomata, K.; Abe, A. *J. Phys. Chem.* **1992**, *96*, 7934.
(40) Tasaki, K.; Abe, A. *Polym. J.* **1985**, *17*, 641.
(41) Smith, G. D.; Jaffe, R. L.; Yoon, D. Y. *J. Am. Chem. Soc.* **1995**, *117*, 530.
(42) Helfand, E. *J. Chem. Phys.* **1978**, *69*, 1010.
(43) Moro, G. *J. Chem. Phys.* **1992**, *97*, 5749.

MA9700340